J Solid State Electrochem (2012) 16:2791–2796
DOI 10.1007/s10008-012-1704-9

ORIGINAL PAPER

A high-performance hybrid supercapacitor with $Li_4Ti_5O_{12}$-C nano-composite prepared by in situ and ex situ carbon modification

Jiangfeng Ni · Liuxiang Yang · Haibo Wang · Lijun Gao

Received: 26 January 2012 / Revised: 19 February 2012 / Accepted: 23 February 2012 / Published online: 8 March 2012

Abstract In this work, we report on the synthesis of in situ and ex situ carbon-modified $Li_4Ti_5O_{12}$-C (LTO-C) nano-composite and its application in a hybrid supercapacitor constructed using activated carbon (AC) and LTO-C nano-composite as positive and negative electrodes, respectively. The hybrid capacitors are characterized by galvanostatic charge–discharge, cycle life testing, and electrochemical impedance spectroscopy. The results reveal that the AC/LTO-C hybrid capacitors exhibit high rate capability and long cycle life. In the potential range of 1.5–3.0 V, the AC/LTO-C hybrid system can deliver a specific capacitance of 83 $F g^{-1}$ based on the total mass of AC and LTO-C electrodes at a current density of 60 mA g^{-1} (2 C rate). At a higher discharge rate of 980 mA g^{-1} (32 C), the capacity is 68 $F g^{-1}$, about 82% of that at 2 C rate. After 9,000 deep cycles at 32 C, the hybrid capacitor still maintains 84% of its initial capacitance. The specific energy of such hybrid system is 20 Wh kg^{-1}, which is at least twice that of an AC/AC system. Combining the high energy density with power capability, the AC/LTO-C hybrid supercapacitor has demonstrated high performance for applications needing high power output.

Keywords Lithium titanate · Activated carbon · Hybrid supercapacitor · Electrochemical performance

Introduction

Electrochemical double-layer capacitor as a power energy storage device, with both electrodes composed activated carbon (AC) material, has characteristics of long cycle life (over 10,000 cycles) and high power density (above 1 kW kg^{-1}) [1]; however, its energy density in comparison with a battery is limited, typically in the range of 5–7 Wh kg^{-1} [2, 3]. Asymmetric hybrid supercapacitors, involving an AC and a battery-type electrode material, have been investigated intensively with an aim of improving energy density while maintaining power robustness and cycle performance [4, 5]. Recently, Li-ion intercalated $Li_4Ti_5O_{12}$ (LTO) has demonstrated favorable characteristics as a promising negative electrode material for power Li-ion batteries [6, 7]. The electrode potential of LTO is 1.55 V vs. Li^+/Li, at which the LTO experiences no SEI film formation on electrode surface in Li^+ ion electrolytes. When combining the LTO-negative with an AC-positive electrode, the LTO/AC constitutes an internal capacitor and battery hybrid system [8, 9]. Its electrode reaction mechanism can be described in the following equations:

$$AC + PF_6^- \leftrightarrows AC^+ PF_6^- + e^- \quad (1)$$

$$Li_4Ti_5O_{12} + 3Li^+ + 3e^- \leftrightarrows Li_7Ti_5O_{12}. \quad (2)$$

However, pristine $Li_4Ti_5O_{12}$ powder is low in electrical conductivity (ca. 10^{-13} S cm^{-1}) [9], which limits its power capability—the key characteristic for supercapacitors. To enhance its conductivity, a great deal of effort has been made by reducing particle size [10, 11], improving the crystallinity [12], doping with heterogeneous atom [13, 14], or modifying particles with carbonaceous materials [15–21]. As a conductivity additive, carbon is considered efficient and cost-effective in enhancing the property of electrode materials [16]. Naoi et al. reported the composite structure material consisting of nano-sized LTO anchored

J. Ni · L. Yang · H. Wang · L. Gao (✉)
School of Energy, Soochow University,
Suzhou 215006, China
e-mail: gaolijun@suda.edu.cn

onto carbon nano-fibers (CNFs); the electrode can be discharged at a rate as high as 300 C [20, 21]. Such work is a major advance for LTO-based hybrid capacitors; however, CNFs could be expensive and the synthesis process could be complex for practical application. In this work, we designed an LTO-C nano-composite modified by both in situ and ex situ carbon. Via a simple sol–gel route, we obtained well-crystallized carbon-coated LTO nanoparticles embedded in a conductive carbon matrix. The in situ carbon from carbonization of organic precursors forms an intimate film on LTO particles to improve the mobility of electrons, while the added ex situ carbon enhances the capacitive behavior of LTO-C by increasing the surface area. The hybrid supercapacitors consisting of AC and LTO-C were fabricated and subjected to various electrochemical measurements. The results show that such an LTO–C/AC hybrid system demonstrates promising electrochemical property in terms of energy density, rate capability, and cycle performance.

Experimental

Synthesis of LTO-C nano-composite

Well-crystallized, both in situ- and ex situ-modified, LTO was prepared via a facile sol–gel route by carefully controlling the synthetic process. Typically, tetrabutyl titanate was first mixed with ethanol with a mole ratio of 1:5 (A solution). Lithium acetate was dissolved into a mixture solution of ethanol/deionized water/acetic acid (B solution). While stirring, B solution was gradually dropped into A solution, resulting in a mixture with total mole ratio of tetrabutyl titanate/lithium acetate/ethanol/acetic acid/deionized water of 1:0.84:10:1.8:4. After stirring for 0.5 h, a certain quality of conductive carbon black (Super-P-Li from Timcal, 35–45 nm in diameter, surface area ~62 $m^2\ g^{-1}$) was added into the clear solution, and after stirring for another 6 h, a black gel was formed. The resulting gelation was dried at 80 °C for 10 h and then annealed at 850 °C for 3 h in N_2 atmosphere. The final LTO-C product contains about 15 wt% carbon as determined by thermal analysis. During the heating process, in situ carbon degraded from organic precursors forms an intimate coating film on LTO particles, while added ex situ carbon acts as both conductive and capacitive additives.

Characterization

The LTO-C electrode was fabricated by laminating LTO-C composite (85 wt%), CMC (2 wt%), SBR (3 wt%), and Super-P-Li-conductive carbon (10 wt%) slurry on an aluminum foil (20 μm). The electrode sheet was dried at 80 °C for 1 h and roll pressed to a thickness of 100 μm. Disks with diameter of 12 mm were pouched out of the laminate to make negative electrodes. An activated carbon (Kuraray YP-50F, Japan) with a surface area of 1,700 $m^2\ g^{-1}$ was used as a positive electrode. The AC electrode was prepared by the same process as the LTO electrode. Both positive and negative electrodes were dried in a vacuum oven at 100 °C for 24 h before being transferred to the glove box.

For Li half cell tests, the LTO-C working electrode was coupled with Li foil as counter and Li wire as reference electrodes in a 1-M $LiPF_6$ in EC/DMC (1:3 in volume) electrolyte and Celgard 2320 as the separator. For the LTO–C/AC hybrid capacitor, the electrolyte was 1 M $LiClO_4$ in propylene carbonate (PC), and the separator was a cellulose paper (TF4035, NKK). All cells were assembled in an argon-filled glove box (MBraun, German). The charge–discharge tests were performed on a LAND battery test system (Jinnuo, China) controlled by a computer at room temperature. Electrochemical impedance spectroscopy (EIS) was performed on an IM6ex impedance facility (ZAHNER, Germany) with an AC perturbation of 5 mV.

Crystallographic structure of the LTO-C composite was identified by X-ray diffraction (XRD) on a D/Max-IIIA diffractometer (Rigaku, Japan) using Cu kα (λ=1.54056 Å) as radiation source. The morphology of the samples was observed using scanning electron microscopy (SEM, FEI Quanta 200F, Netherlands) and high-resolution transmission electron microscopy (HR-TEM, FEI Tecnai G2 T20, Netherlands). X-ray photoelectron spectroscopy (XPS) was carried out on Axis Ultra spectrometer (Kratos, UK) with Al Kr monochromatized X-ray source running at 250 W. The core level binding energies were corrected using the C 1 s binding energy of 284.8 eV. The surface area of the LTO-C material was measured on a ST08 Analyzer (Beifen Instrument, China) using the Brunauer–Emmett–Teller method.

Results and discussion

Physicochemical characterization

X-ray diffraction pattern of the LTO-C composites is shown in Fig. 1a. The XRD result matches well with that of the cubic spinel structure $Li_4Ti_5O_{12}$ (*Fd-3m*, PDF no. 49-0207) and no impurity phase peaks are identified. Diffraction peaks attributed to carbon are invisible in the XRD pattern, possibly due to the amorphous state of conductive carbon. Structural analysis with a Rietveld refinement was conducted on the XRD data, and the result is presented in Fig. 1b. It is seen that the calculated patterns fit well with the observed result, suggesting that the refinement is reliable. The refinement reveals lattice parameter of a=8.356 (2) Å, and corresponding to a unit cell of 583.36 Å, consistent with the standard result (PDF no. 49-0207).

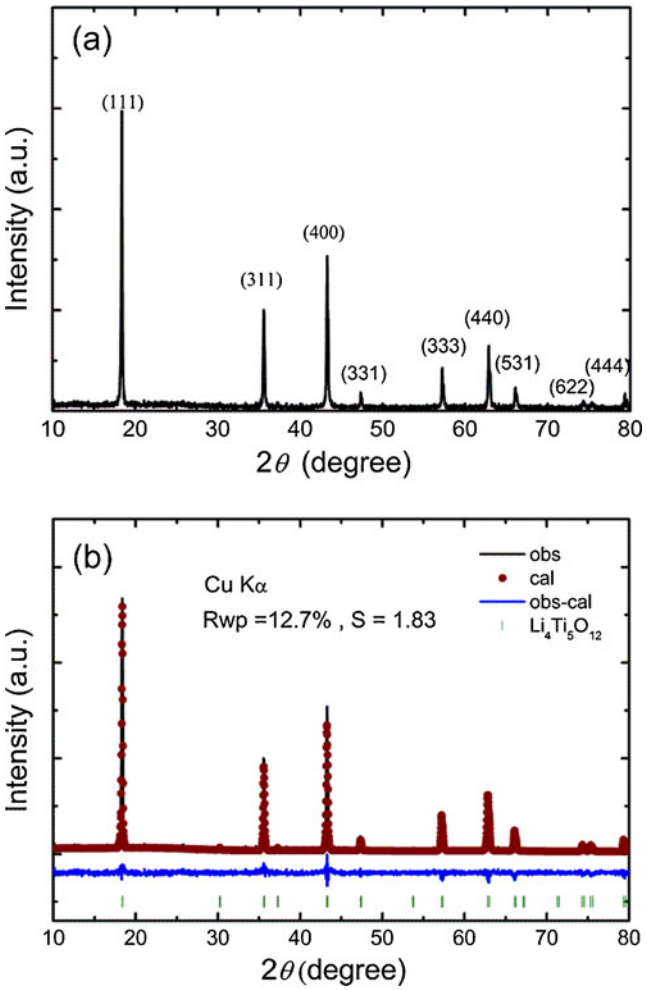

Fig. 1 **a** XRD pattern and **b** Rietveld refinement result of the prepared LTO-C nano-composite

Figure 2a shows the SEM of the LTO-C composite. It can be observed that fine LTO particles with size of 50–150 nm are dispersed in carbon network without obvious agglomeration. The addition of carbon black and in situ-formed carbon effectively prevented the growth of LTO particles during the annealing process. HR-TEM images of the LTO-C composite are presented in Fig. 2b, c, in which LTO nanocrystallites with size of around 20–30 nm embedded in amorphous carbon are clearly observed. A thin amorphous film that may derive from the organic precursor is formed uniformly on the surface of LTO crystallites (Fig. 2c), which is possibly the in situ carbon and thus beneficial for a high electrical conductivity. The LTO crystallites show a lamellar structure with a *d*-spacing of ~0.48 nm, consistent with the (111) peak of XRD pattern of LTO. The result indicates that the added ex situ carbon black involved in the annealing process seems to be not incorporated into the $Li_4Ti_5O_{12}$ lattice, but coherently coated surrounding the crystallites. The N_2 absorption measurement shows that the surface area of LTO-C is 32 m^2 g^{-1}, including contribution from both nano-sized LTO and carbon.

LTO-C/Li cell evaluation

The LTO-C electrode was first investigated by using LTO-C/Li half cells. Figure 3 shows the charge–discharge behaviors of the LTO-C/Li half cell at various rates. The discharge potential at around 1.5 V (against Li^+/Li) is very flat and the gap between charge and discharge plateau is rather narrow, indicating a high Li extraction–insertion kinetics. At a rate of 1 C, the reversible capacity was 168 mAh g^{-1}, very close to the theoretical value of 175 mAh g^{-1} according to reaction (2). Note that the capacity calculation is based on the pure LTO mass only. Even at a charge and discharge rate of 40 C, the reversible capacity can still reach 105 mAh g^{-1}. The rate capability is superior to most previous reports [10–17], which may be attributed to the nano-sized particles and double modification by in situ and ex situ carbon.

When the LTO-C was prepared at 850 °C in the presence of reduction reagents (carbon and organic precursors), partial Ti^{4+} in the surface being reduced to Ti^{3+} is inevitable [22]. Previous research shows intercalation reaction that reaction (2) proceeds in a two-phase manner with narrow solid solution region nearby both end members, while the generation of Ti^{3+} would expand the solid solution domain. The Li diffusivity in solid solution is at least one order of magnitude higher than in two-phase region because Li

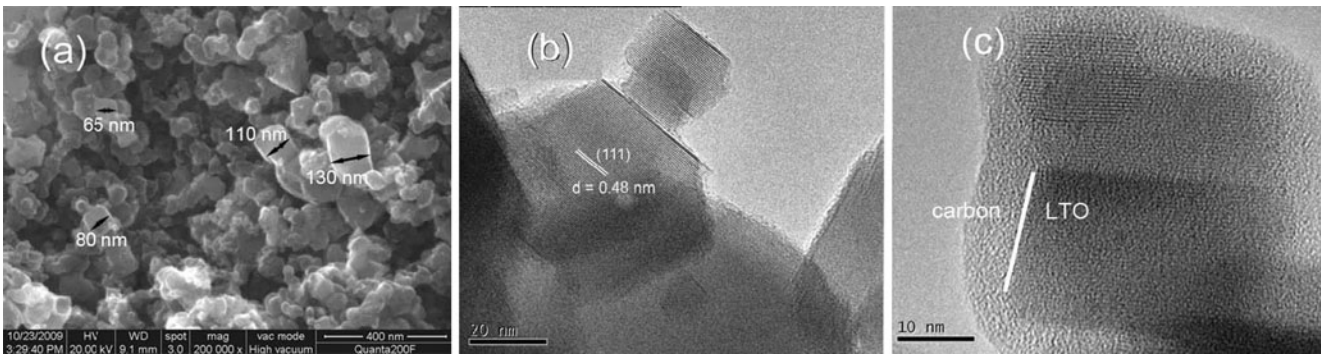

Fig. 2 **a** SEM and **b**, **c** HR-TEM images of the LTO-C nano-composite

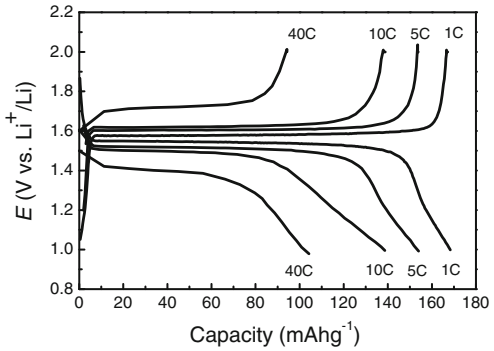

Fig. 3 Charge/discharge behaviors of LTO-C/Li half cell at various rates between 1.0 and 2.0 V

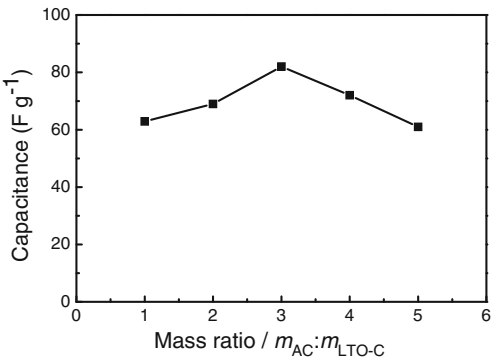

Fig. 5 Specific capacitance as a function of mass ratio of positive against negative materials. The current density is 60 mA g^{-1} and the voltage range is 1.5−3.0 V

diffusion in the latter is retarded by phase boundary movement [17, 23]. Therefore, the kinetics of electrochemical reaction towards Li may be enhanced. Due to relatively low content in the LTO-C sample, the presence of Ti^{3+}-related phase cannot be identified by XRD, but can be detected by XPS. Figure 4 compares the XPS spectra of commercial TiO_2 powder and as-prepared LTO-C. The peak centered at 459 eV can be attributed to Ti 2p, which shift slightly towards low-binding energy side in the pattern of LTO-C. The shift confirms the presence of Ti^{3+} species in the LTO-C sample.

AC/LTO-C hybrid capacitor evaluation

A hybrid capacitor was constructed by using AC-positive and LTO-C negative electrodes in 1 M $LiClO_4$+PC electrolyte. The mass of the electrodes was balanced to fully take profit of the performance of both materials in their optimal working potential range with the principle of $Q_{AC}=Q_{LTO}$. Figure 5 shows the relationship between mass ratio of positive to negative materials and the specific capacitance at a selected current rate of 60 mA g^{-1}. It is obvious that the specific capacitance increases with the increase in mass ratio of positive/negative materials until $m_{AC}/m_{LTO}=3:1$, where a maximum value is reached. This value departs from the 4:1 ratio based on the theoretical-specific capacity of LTO and AC; it is possibly due to the added ex situ carbon in LTO electrode. The rate capability of such a mass-balanced LTO-C/AC hybrid cell was examined at various discharge rates as shown in Fig. 6. With the increase of current rate, the discharge time reduces while the profile almost remains. At a rate of 980 mA g^{-1} (about 32 C), the discharge time is 1 min in the voltage range of 3.0−1.5. For comparison, the charge–discharge profile at 60 mA g^{-1} (2 C) is presented in the inset of Fig. 6. The voltage profile declines with time as a capacitor should be; however, the slope is not strictly linear. The results indicate that the hybrid capacitor exhibited discharge characteristics of the combination of a capacitor and a battery [24].

Table 1 summarizes the specific capacitance of such AC/LTO-C hybrid capacitor at various currents. The discharge specific capacity C_m was calculated by the following formula:

$$C_m = \frac{i \times \Delta t}{m \times \Delta V} \quad (3)$$

where i (in amperes) stands for the discharge current, ΔV (in volts) the discharge voltage change (exclude the iR drop), and Δt (in seconds) the discharge time consumed in the voltage

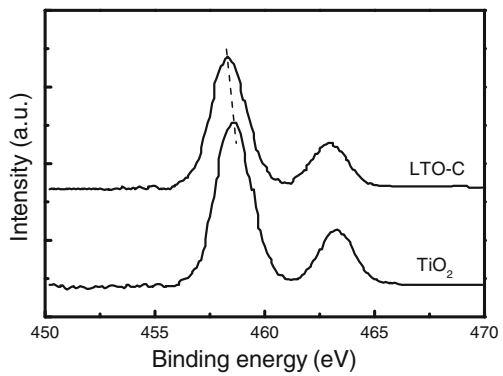

Fig. 4 XPS spectra of TiO_2 powder and the LTO-C nano-composite

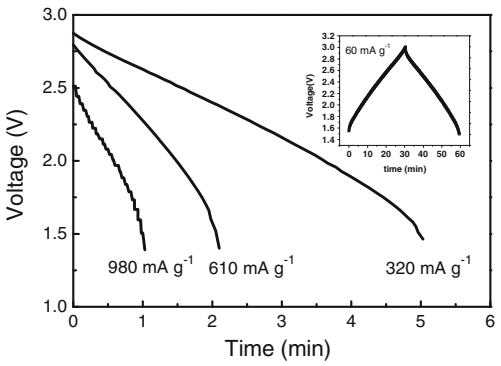

Fig. 6 Rate discharge behaviors of the LTO-C/AC hybrid capacitor between 1.5 and 3.0 V. Inset shows charge–discharge profile at current density of 60 mA g^{-1} for clarification

Table 1 Specific capacitance based on different electrode material weights of the AC/LTO-C hybrid capacitor at various discharge currents

Current density (mA g^{-1})	60	320	610	980
LTO-C electrode (F g^{-1})	337	334	323	271
AC electrode (F g^{-1})	111	108	105	90
Both electrode (F g^{-1})	83	82	79	68
AC/LTO-C hybrid capacitor (F g^{-1})	22	21	20	18

change range of ΔV. The mass used in calculation involves that of LTO-C single electrode, AC single electrode, active material of both electrodes, and the entire hybrid capacitor (including both electrode materials, current collectors, electrolyte, and separator). With the increase of discharge current from 60 to 980 mA g^{-1}, the specific capacitance of the LTO-C electrode decreases slowly from 83 to 68 Fg^{-1}, while that of the hybrid capacitor (based on the entire mass of the capacitor), it drops from 22 to 18 Fg^{-1}, only fading 18%. The rate test results suggest that the hybrid capacitor possesses an excellent rate capability. Since the AC material is known to be high rate capable based on its principle of ion diffusion in double layer, the rate performance of the hybrid is dominated by the Li^+ diffusion rate in the lattice of intercalation LTO compound. Since LTO is a zero-strain material, when its particle size is made small (100–150 nm in this case) and its electron and ion mobility is improved by adding conductive carbon and by generation of Ti^{3+} species, high rate performance of the LTO-C/AC hybrid cell has been realized. It is worth pointing out that the embedded carbon also plays an importance role in enhancing the capacitive behavior of the LTO-C anode.

The specific energy was calculated from $E=1/2\ C_m(V_2^2-V_1^2)$, where V_2=3.0 V−iR and V_1=1.5 V. The specific power was obtain from $P=E/t$, where t is the time duration for the capacitor to discharge from V_2 to V_1. It should be noted that this specific power is an average performance value which differs from that of the maximum power of "matched resistance," $P_{max}=V^2/4R$. Such a data is more reliable since it is a power performance of the hybrid capacitor device measured through the full discharge duration. The result demonstrates that the specific energy is 20 Wh kg^{-1} at a power density of 37 Wkg^{-1}; when the power output reaches 440 Wkg^{-1}, the specific energy retains at 16 Wh kg^{-1} for the entire AC/LTO-C hybrid capacitor system. The energy density is at least twice that of a conventional AC/AC system [1], and comparable with results of other hybrid capacitors [9, 25]. Therefore, it may find application in many fields needing high power.

The cycle life results of the AC/LTO-C hybrid capacitor at charge–discharge current of 980 mA g^{-1} are shown in Fig. 7. The hybrid cell displayed a sustained stability over a

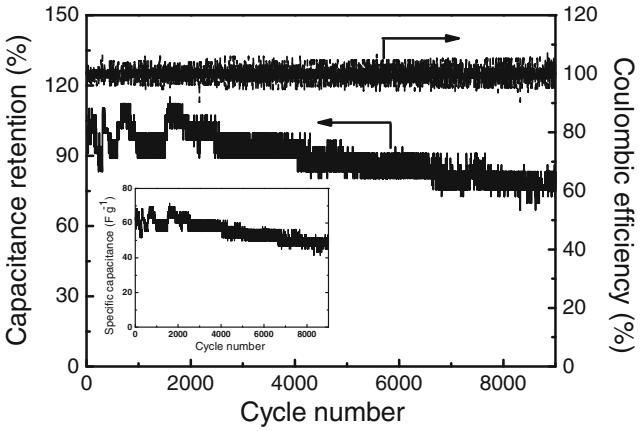

Fig. 7 Capacity retention and coulombic efficiency of the LTO-C/AC hybrid capacitor at a current density of 980 mA g^{-1}. *Inset* shows the profile of specific capacitance vs. cycle number

fairly long cycle time at such a high cycle rate. After 9,000 cycles, the specific capacitance retains 84% of the initial value, and the coulombic efficiency is close to 100%.

To understand the excellent cycling property of the LTO-C/AC hybrid capacitor, EIS experiments were carried out at different stages, i.e., before cycling, and after 3,000 and 9,000 cycles. As shown in Fig. 8, the Nyquist plots of the impedance spectra consist of two components: a semi-circle in high frequency and a straight line in low frequency. In the high frequency region, the diameter of the semi-circle represents the resistance (R_{ct}) related to the charge transfer across the electrode interface, whereas the low frequency straight line represents the Li diffusion in the electrodes. The straight line deviates from vertical shape, indicating that ion diffusion in the electrode is not a pure capacitive behavior [26]. The high frequency intercept of the semi-circle on the real axis yields the internal resistance (R_s). An increase of R_s and R_{ct} can be observed after the cell being cycled. The former is presumably caused by the increasing electrode/electrolyte contact resistance, while the latter is due to the decrease in the area of electrodes induced by repeated

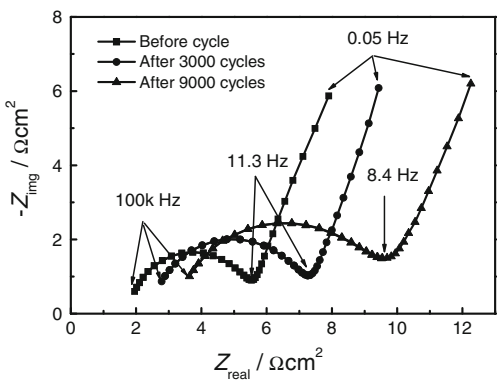

Fig. 8 Electrochemical impedance spectra of the AC/LTO-C hybrid capacitor at different stages

expansion and contraction during the cycles. It is seen that the increase of both R_s and R_{ct} is not severe throughout the cycling process, which explains the stable capacity delivery capability of the LTO-C/AC hybrid upon cycling [27].

Conclusion

In summary, the in situ and ex situ carbon-modified LTO-C nano-composite was directly synthesized via a sol–gel method. The LTO-C nano-composite was used as a negative electrode coupled with AC-positive electrode to construct the AC/LTO-C hybrid capacitor. Electrochemical measurement results reveal that the AC/LTO-C hybrid capacitors exhibit high rate performance and long cycle life. In the voltage range of 1.5−3.0 V, the hybrid cell can deliver a specific energy of 20 Wh kg^{-1} at the specific power of 37 Wkg^{-1}, which is a significant improvement in energy density over that of an AC/AC system. When discharged at 440 Wkg^{-1} power, the specific energy remains at 16 Wh kg^{-1}. Cycle performance test on the hybrid cell shows the capacity can hold 84% of its initial value after 9,000 deep cycles at a 980 mA g^{-1} (a 32 C rate). It is believed that the double-carbon modification enhances the conductivity, reduces the particle size, assists in the formation of Ti^{3+} species, and increases the capacitance of the LTO-C material, which enables the high rate and stable cycle performance of the LTO-C/AC hybrid capacitor.

Acknowledgments Financial support of National 863 Project (No. 2011AA11A235) is gratefully acknowledged.

References

1. Conway BE (1999) Electrochemical supercapacitors: scientific fundamentals and technological applications. Kluwer Academic/Plenum, New York
2. Kotz R, Carlen M (2000) Electrochim Acta 45:2483–2498
3. Burke AF (2007) Electrochim Acta 53:1083–1091
4. Amatucci GG, Badway E, Pasquier AD, Zheng T (2001) J Electrochem Soc 148:A930–A939
5. Yu N, Gao L, Zhao S, Wang Z (2009) Electrochim Acta 54:3835–3841
6. Stewart S, Albertus P, Srinivasan V, Plitz I, Pereira N, Amatucci G, Newman J (2008) J Electrochem Soc 153:A253–A261
7. Yang L, Gao L (2009) J Alloys Comp 485:93–97
8. Du Pasquier A, Plitz I, Gural J, Menocal S, Amatucci GG (2003) J Power Sources 113:62–71
9. Cheng L, Liu HJ, Zhang JJ, Xiong HM, Xia YY (2006) J Electrochem Soc 153:A1472–A1477
10. Jiang C, Ichihara M, Honma I, Zhou H (2007) Electrochim Acta 52:6470–6475
11. Kalbáč M, Zukalová M, Kavan L (2003) J Solid State Electrochem 8:2–6
12. Liu P, Sherman E, Verbrugge M (2010) J Solid State Electrochem 14:585–591
13. Jhan Y-R, Lin C-Y, Duh J-G (2011) Mater Lett 65:2502–2505
14. Qi Y, Huang Y, Jia D, Bao SJ, Guo ZP (2009) Electrochim Acta 54:4772–4776
15. Wang GJ, Ga J, Fu LJ, Zhao NH, Wu YP, Takamuro T (2007) J Power Sources 174:1109–1112
16. Yuan T, Yu X, Cai R, Zhou Y, Shao Z (2010) J Power Sources 195:4997–5004
17. Wang Y, Liu H, Wang K, Eiji H, Wang Y, Zhou H (2009) J Mater Chem 19:6789–6795
18. Zhao L, Hu Y-S, Li H, Wang Z, Chen L (2011) Adv Mater 23:1385–1388
19. Zhu N, Liu W, Xue M, Xie Z, Zhao D, Zhang M, Chen J, Cao T (2010) Electrochim Acta 55:5813–5818
20. Naoi K, Ishimoto S, Isobe Y, Aoyagi S (2010) J Power Sources 195:6250–6254
21. Naoi K (2010) Fuel Cells 10:825–833
22. Kellerman DG, Gorshkov VS, Shalaeva EV, Tsaryev BA, Vovkotrub EG (2012) Solid State Sci 14:72–79
23. Chen YC, Ouyang CY, Song LJ, Sun ZL (2011) Electrochim Acta 56:6084–6088
24. Conway BE (1991) J Electrochem Soc 138:1539–1548
25. Du Pasquier A, Plitz I, Menocal S, Amatucci G (2003) J Power Sources 115:171–178
26. Li Y, Zijll M, Chiang S, Pan N (2011) J Power Sources 196:6003–6006
27. Dandekar MS, Arabale G, Vijayamohanan K (2005) J Power Sources 141:198–203